Appl Magn Reson (2010) 37:819–832
DOI 10.1007/s00723-009-0088-1

Applied
Magnetic Resonance

Variable Coupling Scheme for High-Frequency Electron Spin Resonance Resonators Using Asymmetric Meshes

D. S. Tipikin · K. A. Earle · Jack H. Freed

Received: 3 July 2009 / Published online: 13 November 2009

Abstract The sensitivity of a high-frequency electron spin resonance (ESR) spectrometer depends strongly on the structure used to couple the incident millimeter wave to the sample that generates the ESR signal. Subsequent coupling of the ESR signal to the detection arm of the spectrometer is also a crucial consideration for achieving high spectrometer sensitivity. In previous work, we found that a means for continuously varying the coupling was necessary for attaining high sensitivity reliably and reproducibly. We report here on a novel asymmetric mesh structure that achieves continuously variable coupling by rotating the mesh in its own plane about the millimeter-wave transmission-line optical axis. We quantify the performance of this device with nitroxide spin label spectra in both a lossy aqueous solution and a low-loss solid-state system. These two systems have very different coupling requirements and are representative of the range of coupling achievable with this technique. Lossy systems, in particular, are a demanding test of the achievable sensitivity and allow us to assess the suitability of this approach for applying high-frequency ESR, e.g., to the study of biological systems at physiological conditions. The variable coupling technique reported on here allows us to readily achieve a factor of ca. 7 improvement in the signal-to-noise ratio at 170 GHz and a factor of ca. 5 at 95 GHz over what has previously been reported for lossy samples.

D. S. Tipikin · K. A. Earle · J. H. Freed (✉)
Department of Chemistry and Chemical Biology, Cornell University,
Ithaca, NY 14853, USA
e-mail: jhf3@cornell.edu

K. A. Earle
Physics Department, University at Albany (SUNY), 1400 Washington Ave.,
Albany, NY 12222, USA

1 Introduction

The development of high-frequency electron spin resonance (ESR) over the past two decades is driven mainly by the desire to achieve improved *g*-factor resolution [1], and time-scale resolution of internal and overall motion of macromolecules spin-labeled by nitroxides [2–5]. This broad range of applications indicates the need for a spectrometer of flexible design that can accommodate samples with very different properties under a variety of conditions. Due to the generally lower available powers as the millimeter wave frequency increases [6], there is a need for efficient transmission lines to connect the source, the sample and the detector. A number of creative approaches to the problem of low millimeter wave power have been explored. For example, fundamental and overmoded waveguides have been used in high-frequency ESR spectrometers [7–9]. Fundamental-mode waveguide becomes progressively lossier per unit length as the frequency increases. Overmoded waveguide does not have this defect, but it is more susceptible to mode conversion losses. Given that high-frequency ESR usually requires concomitantly large magnetic fields, since the electron Zeeman resonance frequency is proportional to the applied field, transmission lines extending over hundreds or thousands of wavelengths are required when a superconducting magnet is used to generate the applied field, due to the high degree of temperature isolation required to bring the magnet to operating temperature.

Transmission lines based on quasioptical techniques are a useful alternative to waveguide-based transmission lines as the frequency increases. The quasioptics approach is based on a well-defined approximation that incorporates diffraction effects, resulting in design formulas that are almost as easy to use as simple geometrical optics formulas [6]. The application of quasioptical techniques to high-frequency ESR was introduced by Freed and co-workers [10], and is becoming increasingly popular in other high-frequency ESR groups, particularly for frequencies above 100 GHz [11–16]. To date, high-field ESR spectrometers based on quasioptical techniques have been operated in transmission [10, 13], reflection [11–13] and induction [11, 12, 14, 15] modes.

The induction mode exploits the preferred absorption via the ESR effect of circularly polarized radiation. A linearly polarized millimeter wave that is incident on an ESR-active sample reflects and transmits an elliptically polarized beam. The reflected signal can be analyzed into components co- and cross-polarized with respect to the incident beam. The co-polarized response is the response that can be duplexed in a waveguide-based reflection spectrometer. For a reflection-mode spectrometer, isolation of the transmit and receive arms is a crucial design consideration that must be carefully optimized in order to have a high sensitivity device. Smith et al. [12] have shown that the magnitude, but not the phase, of the ESR signal is the same in the co- and cross-polarized channels.

Quasioptical techniques allow one to duplex the cross-polarized response, which is ideally orthogonal to the excitation. Given that limiters are not readily available at higher frequencies, this technique of polarization duplexing was crucial for protecting our receiver from pulse feedthrough in our 95 GHz pulse/continuous-wave (cw) spectrometer [4]. In that work, we introduced a variable coupling scheme that was designed to be symmetric in the co- and cross-polarized response. With this novel arrangement, we were able to achieve critical coupling for a variety of samples: lossy and non-lossy. The symmetric double-mesh variable-coupling scheme is based on a spring-loaded mechanism whose performance degrades as the sample temperature varies. Furthermore, its delicate design makes it susceptible to mechanical vibration. In order to investigate alternative coupling structures with more robust mechanical characteristics, we experimented with a variety of mesh configurations that would provide continuously variable coupling with good temperature-independent performance and without the need for a delicate mechanical tuning mechanism. Our experimentation led us to develop an asymmetric mesh suitable for use in an induction-mode spectrometer that is the quasioptical analog of an elliptical iris (R. Mett, Medical College of Wiconsin, Milwaukee, Wisconsin, USA, pers. commun.). Previous designs at 170 and 240 GHz [3] had used a single, square symmetric mesh, where it was assumed that the impedance was independent of the relative orientation of the polarization and the symmetry axes of the grid. In practice, we found that working with symmetric, fixed grid parameters made critical coupling a 'hit-or-miss' affair (i.e., for each sample one would have to explore a range of meshes with different grid parameters until a near-critical coupling could be achieved. Then fine adjustment can be made by rotating the square mesh). What was needed was a way to combine the mechanical robustness of the single mesh design with the variability of the two-mesh design introduced at 95 GHz [4].

The asymmetric mesh approach has the advantage that it can withstand repeated temperature cycling and can be employed with all of our spectrometers based on quasioptical propagation techniques. These instrumentation advances are especially important for the study of nitroxide spin-labeled biological samples, in order to resolve the complicated spectra that result from the interplay of internal motions of the macromolecule, including motions of the tether by which the nitroxide is attached to the macromolecule, as well as the overall tumbling of the macromolecule. Analysis of ESR spectra at more than one frequency is a useful tool for accomplishing this program [1, 5, 17]. Since spectra need to be collected under a variety of conditions at different frequencies, it is important that the spectrometer is operable under a broad range of experimental conditions, consistent with high sensitivity.

If the system is dominated by detector noise and carrier feedthrough does not set a limit on the system dynamic range, one could, in principle, just use a more powerful source to improve the signal-to-noise ratio (SNR). For many applications, however, the output power of millimeter wave sources is limited, as we have noted, and thus optimizing the coupling is the best means for improving sensitivity. We use an open Fabry-Pérot resonator (FPR) in a semi-confocal configuration. The asymmetric mesh serves as the coupling device and as the flat mirror of the semi-confocal FPR. The general outline of the FPR is shown in Fig. 1.

Frequency tuning is accomplished by varying the separation of the curved mirror and the coupling mesh. We have found that it is important to allow the position of the sample to vary in the resonator in order to position the sample in a region that minimizes dielectric losses and, thus, maximizes the quality factor of the FPR. Due to the 'interleaved' standing-wave mode structure of an FPR [18], this minimum loss position is typically a minimum of the millimeter wave electric field and a

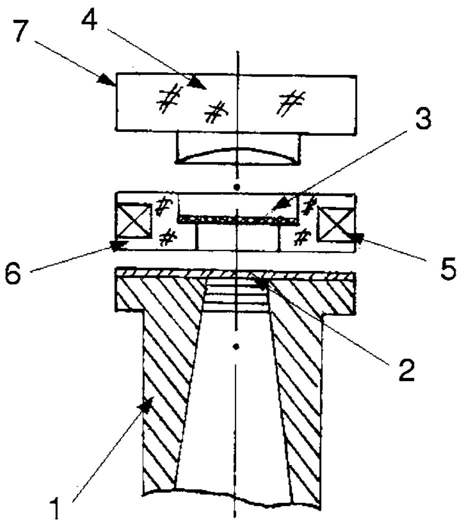

Fig. 1 Sectional view of a high-frequency semi-confocal Fabry-Pérot resonator. *1* Beam waist reducing corrugated waveguide taper, *2* coupling mesh, *3* sample, *4* curved mirror, *5* modulation coil, *6* sample holder, *7* support structure for curved mirror

maximum of the millimeter wave magnetic field. As the fields are displaced from the beam waist, diffractive beam growth in the FPR causes the equiphase surfaces, defining the millimeter wave fields, to become progressively more curved. We have determined experimentally that the optimum lossy sample position is not directly on the coupling structure but displaced slightly from it, approximately an integral number of half wavelengths away from the flat mirror, in a region of the resonator where the phase front of the millimeter wave is still nearly planar [19]. For lossy samples, we have developed a sample geometry that is similar to the flat cell geometry common at X-band, but adapted to the particular requirements of the millimeter wave field geometry [19]. Basically, lossy samples are configured as a very thin disk with the plane of the disk perpendicular to the optical axis of the FPR.

In order to analyze this situation in a tractable way, we may use well-known concepts from transmission line theory [6, 20]. For this analysis, we shall approximate a quasioptical transmission line as a uniform transmission line and neglect diffractive beam growth. In the neighborhood of the beam waist, where the radius of curvature is large, this is an excellent approximation [6]. Indeed, we find that for field points far from the beam waist, but still in the paraxial region, where displacements from the optical axis are small, the phase front curvature is significant and dielectric losses are large, due to penetration of the electric field into the sample. Thus, in the near field of the beam waist, where the beam may be thought of as approximately planar, we parameterize the behavior of the resonator by a complex load impedance Z_L [21]. The transmission line has a characteristic impedance Z_S, which we may take to be the impedance of free space at the beam waist. The actual value is a matter of convention as it is only ratios of impedances that are physically significant. The power reflected from the load (or resonator) is proportional to $|\rho_{in}|^2$, where ρ_{in} is the voltage reflection coefficient:

$$\rho_{in} = (Z_L - Z_S)/(Z_L + Z_S).$$

Note that when $Z_L = Z_S$, the reflection coefficient ρ_{in} and the reflectivity $\Gamma = |\rho_{in}|^2$ vanish and all of the available power from the source is dissipated in the resonator. When this condition is achieved, the resonator is said to be critically coupled.

2 Analysis

For detailed analysis of the coupling, it is convenient to use the 'ABCD' transmission line matrix method [21]. The scheme for the analysis is shown in Fig. 2. According to this scheme, the input voltage and current may be related to the output voltage and current for any transmission line element, such as a mesh shunting the transmission line, by two coupled linear equations $V_{in} = AV_{out} + BI_{out}$, $I_{in} = CV_{out} + DI_{out}$. In matrix form, one has

$$\begin{bmatrix} V_{in} \\ I_{in} \end{bmatrix} = \begin{bmatrix} A & C \\ B & D \end{bmatrix} \begin{bmatrix} V_{out} \\ I_{out} \end{bmatrix}.$$

In an optical (or quasioptical) element train, one may compute the system response by multiplying 'ABCD' matrices appropriate for each element in the train. This procedure works because the input voltage and current column matrix at a given element is the output of the prior stage. Thus, once the 'ABCD' matrices for individual elements are known, the system response may be found from straightforward matrix multiplication. An example of this procedure for the ESR case is given elsewhere [21]. For the present purpose, we consider the corrugated waveguide with a beam waist reducing output taper as the source. The resonator, except for the coupling mesh, is taken as the load. We will define Z_S as the (complex) impedance of the source and Z_L as the (complex) impedance of the load. The coupling mesh can be described as a shunt element with admittance Y_M:

$$\begin{bmatrix} A & B \\ C & D \end{bmatrix} = \begin{bmatrix} 1 & 0 \\ Y_M & 1 \end{bmatrix}.$$

For a wire grid with shunt impedance $Z_M = 1/Y_M$, the voltage reflection coefficient is equal to

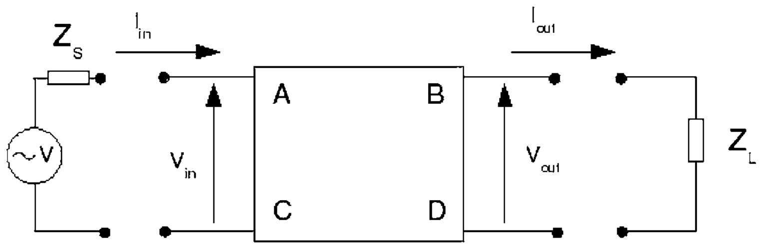

Fig. 2 A section of transmission line in terms of its ABCD representation. The figure shows the conventions for the senses of the input and output voltages and currents. In order to have a complete description, it is necessary to specify the source and load impedances

$$\rho_{in} = \frac{(AZ_L - DZ_S + B - CZ_LZ_S)}{AZ_L + DZ_S + B + CZ_LZ_S}.$$

The resonator is critically coupled, i.e., $\rho_{in} = 0$, for $A = D = 1$, $B = 0$, $Y_M = 1/Z_M$ when:

$$Z_M = Z_LZ_S/(Z_L - Z_S). \quad (1)$$

It is important to note that the impedances and reactances used here are complex numbers. Thus, in order to reach critical coupling, there must be enough flexibility in the coupling scheme that the real and imaginary parts of ρ_{in} vanish separately. Given that the only degree of freedom is the orientation of the mesh in its plane of rotation, it is difficult to satisfy Eq. (1) exactly. In practice, one finds that one can only minimize $|\rho_{in}|$. Thus, there will almost always be a small amount of leakage power reflected back to the source. For a one-dimensional grid, Goldsmith [6] has shown that the reactance varies by almost three orders of magnitude, when the grid is rotated from an orientation parallel to the one perpendicular to the *E*-field. For a rectangular grid, where the polarization response is assumed to be superposable, there is a smooth variation of the reflectivity whose limits are set by the aspect ratio of the grid geometry. We have found experimentally that a mesh with the 'brick wall' geometry, with an aspect ratio of 3:1 (see below), provides enough of a coupling range to allow us to achieve a useful level of spectrometer performance for both lossy and non-lossy samples.

In order to develop criteria for achieving optimal coupling (in the sense of minimization of back reflected power), we compared the performance of different types of meshes used as the flat mirror in the resonator. These developmental studies were done at 170 GHz. We summarize the results of our experiments at 95 and 240 GHz in Sect. 6. The first mesh used was a square mesh with a period of 1 mm. For this mesh, the width of the metal strips was 1/3 mm. This mesh is shown as 1 in Fig. 3. Asymmetric meshes with aspect ratios as shown in Fig. 3 (meshes 2 and 3) were also studied.

For these experiments, it is important to note that significant Lorentz forces are generated by magnetic field modulation-induced eddy currents in the mesh coupling structure at the Larmor field of 6 T. It is, therefore, essential to choose a mesh material that is mechanically rigid. Due to the short wavelength of the millimeter wave radiation, it is also necessary to ensure that the thickness of the mesh is small compared to a wavelength, as an electrically thick mesh would have a more complicated orientation dependence due to waveguide effects. In addition, the mesh material must have sufficiently good conductivity that high reflectivity can be achieved. These constraints are difficult to satisfy simultaneously. After some experimentation, we determined that laser-cut, gold-plated, stainless steel meshes with a thickness of 0.005 in. satisfied the constraints of rigidity, conductivity and thickness (recall: 1 mm = 0.0397 in.). The stainless steel meshes were prepared for us by the Rache Corporation (http://www.rache.com).

To investigate the coupling properties of the meshes, the following experiment was performed. A particular polarization of the *E*-field of the input beam with respect to the mesh symmetry axis (at normal incidence) was chosen and fixed. For the symmetric

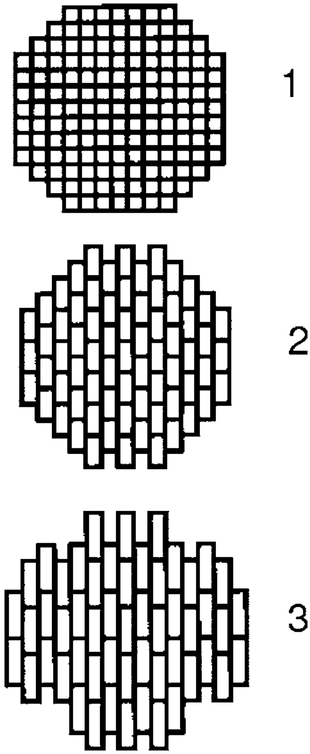

Fig. 3 Geometries of the meshes studied in this work. *1* Symmetric mesh. This corresponds to the original configuration discussed in Ref. [3]. *2* Asymmetric 'brick wall' mesh with 2:1 aspect ratio. *3* Asymmetric 'brick wall' mesh with a 3:1 aspect ratio. This style of mesh gave the most useful level of performance in practice. The mesh parameters are discussed in the text

square mesh, the polarization axis was chosen arbitrarily with respect to one of the grid axes. Subsequent measurements at different orientations were referred to the same grid axis. For the symmetric and asymmetric meshes, the resonator was tuned by optimizing the position of the curved reflecting mirror and the position of the sample within the resonator. The ESR spectrum was then recorded. Without varying the position of the curved mirror, or the sample, the relative orientation of the incident polarization and the mesh was then varied. ESR spectra were recorded for each new orientation. Both the amplitude of the signal and the phase of the signal were then analyzed as a function of the relative angle. The reliability of the experimental procedure was enhanced by performing the initial tuning at an orientation where the signal was strong. This initial orientation defined a reference angle zero as discussed below.

Two samples were studied: a lossy, 1.0 μl aqueous solution of 4-hydroxy-2,2,6,6-tetramethylpiperidine-N-oxyl (OH-TEMPO, 2.5 mM) and a non-lossy solid sample of nitroxide spin label suspended in dried starch. The dried starch sample was prepared by mixing dry starch with a 10 mM OH-TEMPO water solution and air drying at room temperature for 1 day. The fluid, aqueous sample was in the motional narrowing regime, and the non-lossy, solid sample was in the rigid limit. Spectra for both samples were collected at ambient temperature. Typical spectra are shown in Fig. 4. The dried starch spectrum shown in Fig. 4 shows the presence of Mn^{2+} due to impurities in the starch, but this additional signal does not influence the analysis of the mesh behavior.

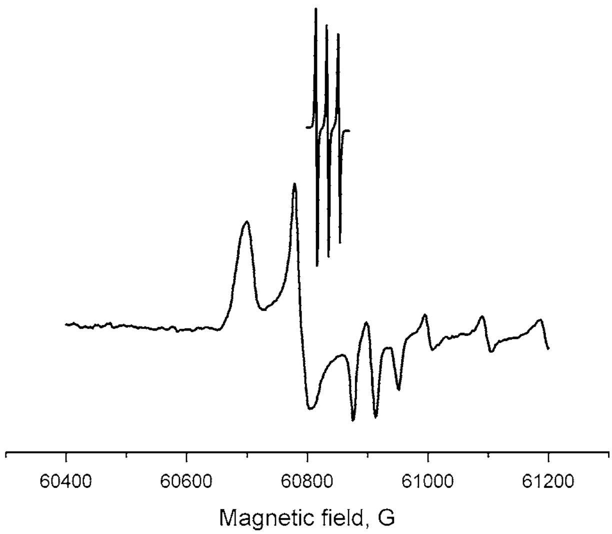

Fig. 4 Typical derivative absorption spectra at 170 GHz. The *upper trace* shows a motionally narrowed nitroxide spectrum of OH-TEMPO in water. The *lower trace* was obtained from a suspension of nitroxide spin label in a low-loss starch matrix. Note the Mn(II) impurities on the high-field side of the *lower trace*

As a result of varying the incident polarization angle, the phase of the signal was changed from pure absorption to a mixture of absorption and dispersion. Extraction of the pure absorption signal was accomplished using a locally written program for phase correction. The phase correction relies upon the fact that the absorption and dispersion signals are related by a Hilbert transform. The phase correction program uses Matlab to compute the Hilbert transform of the observed signal. The proper phase is then chosen by varying the admixture of the original signal and its Hilbert transform [21]. In order to gain a better understanding of this procedure, one may represent the experimentally observed signal S as follows:

$$S = aA + bH(A), \tag{2}$$

where a and b are weight coefficients determined by the experimental conditions. Here, A is the desired pure absorption and $H(A)$ is defined as the Hilbert transform of A.

After applying the Hilbert transform to the signal, recalling that $H(H(S)) = -S$, we have

$$H(S) = aH(A) - bA. \tag{3}$$

The program then multiplies Eq. (2) by cos θ and Eq. (3) by sin θ (where θ can be chosen arbitrarily in the range 0°–360°), and subtracts Eq. (3) from Eq. (2). One finds

$$S\cos\theta - H(S)\sin\theta = (a\cos\theta + b\sin\theta)A + (b\cos\theta - a\sin\theta)H(A). \tag{4}$$

The value of θ is varied until the absorption component of the spectrum is maximized. We note that the optimum value of θ may be a function of spectral position due to the resonator drift. By using Eq. (4), we are able to determine the spectral phase with sufficient accuracy for our experiments. It is worthwhile mentioning that the phase obtained in this manner is consistent with that inferred from more conventional methods [22].

3 Non-Lossy Samples: Symmetric Mesh

The behavior of the phase and the amplitude of the absorption for the non-lossy sample are shown in Fig. 5. In order to simplify the presentation, only the amplitude of the absorption is plotted. It is interesting to note that the measured response of the square mesh is, in fact, anisotropic, despite the apparently reasonable expectation that the response should be isotropic. In fact, both amplitude and phase change as a function of relative orientation. The phase response shows two different behaviors, a stable region, from −30° to +60°, which we will call region 1, and a narrower, unstable region, from 80° to 130°, which we will call region 2. The response varies from a maximum in regions of phase stability (region 1) to a minimum in regions of phase instability (region 2). The experimentally relevant region is the stable region, where the SNR is a maximum.

We attribute the amplitude change in the stable region to changes in the coupling mesh impedance. In our view, the phase stability is due to two effects. The first is the suppression of spurious modes by the position of the sample and the curved mirror. The second is due to the variability of the polarization profile across the Gaussian beam as the beam waist is varied [6]. Open resonators are known to have a variety of radial and azimuthal modes, which can be selected by varying the position of the tuning mirror [6, 19]. Due to the dispersive nature of the spurious radial and azimuthal modes, we attribute the low amplitude and unstable phase of region 2 to mesh orientations that excite several nearly degenerate modes with different

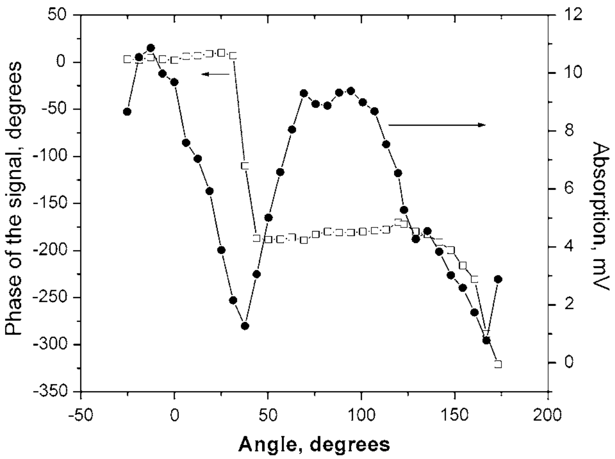

Fig. 5 Plot of peak derivative absorption (*filled circles*) and signal phase (*open squares*) as a function of mesh orientation for the non-lossy sample of Fig. 4. The mesh used for these experiments was the symmetric mesh (number 1) shown in Fig. 3

millimeter wave phases. We note that when the spectrometer response as a function of frequency is displayed on an oscilloscope, conditions corresponding to region 1 lead to clearly observed tuning resonances. We call this the optimal coupling region. At a certain angle in region 1, a signal maximum is achieved, corresponding to maximum millimeter wave B_1 and minimum back reflected power. We call regions of unstable phase (region 2) the mode-coupling regions. In these regions, the mesh–mirror–sample configuration allows the excitation of several nearly degenerate modes, as discussed above, with low SNR. For accurate work, the mode-coupling region should be avoided. We speculate further on the effects of a position-dependent polarization profile in Sect. 6.

4 Non-Lossy Samples: Asymmetric Meshes

The maximum SNR corresponding to the square mesh was measured to be 1195, while the maximum SNR corresponding to the asymmetric mesh was found to be 8350. This gives a SNR enhancement of 7:1 for the asymmetric mesh compared to the symmetric mesh. Given that the noise amplitude is comparable for the two meshes, the SNR enhancement is roughly proportional to the change of the signal amplitude for the asymmetric mesh, compared to the symmetric mesh. These observations were supported by investigations on several samples.

5 Lossy Samples

The phase and amplitude dependence for mesh number 3 and 2.5 mM TEMPO in water is shown in Fig. 6. Although they are not as pronounced as in Fig. 5, there are still regions of relative phase stability (−50°–40°, 70°–130°, 160°–230°) and regions of phase instability (40°–70°, 130°–160°). Given that the borders between regions 1 and 2 are now less clear, the numerical values of degrees in parentheses include some rounding to the nearest angular decade. In the mode-coupling region, the signal is weak, while in the regions of optimal coupling it is strong and reaches a maximal value, which is much larger than the optimum obtainable for the square mesh previously used. The SNR enhancement is comparable to what we achieved in the non-lossy case, i.e., approximately 7:1. We attribute this to the broader range of coupling achievable with the asymmetric mesh, according to Eq. (1). Better coupling means higher resonator conversion efficiency, and, thus, a stronger signal in the absence of spectral saturation [15]. We found that an angle of ~60° in Fig. 6 corresponds to the E-field, being parallel to the long (continuous) axis of mesh number 3.

We speculate that the violation of twofold symmetry displayed by the values of the maxima in Fig. 6 at ~10° and ~200° is due to some misalignment of the bridge. It is known, e.g., that corrugated waveguide, although nominally cylindrically symmetrical, has an orientation-dependent reflectivity [19]. The likeliest mechanisms are that the beam waist is slightly off center with respect to the transmission-line optical axis or that the corrugated waveguide actually has a

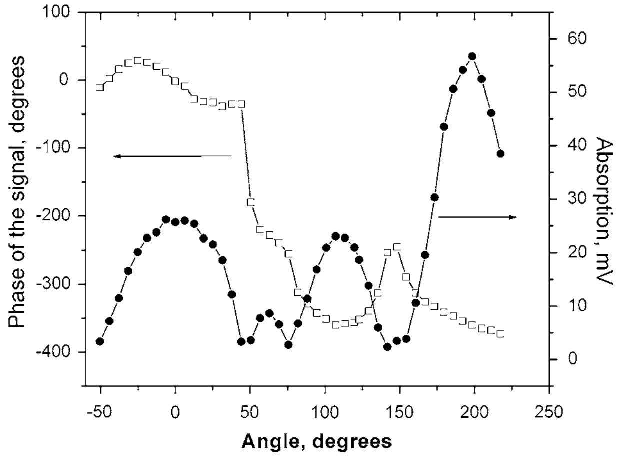

Fig. 6 Plot of peak derivative absorption (*filled circles*) and signal phase (*open squares*) as a function of mesh orientation for the lossy sample of Fig. 4. The mesh used for these experiments had the 3:1 brick wall geometry shown in Fig. 3

slightly elliptical cross-section. When the *E*-field is almost parallel to the long axis of the mesh, the reflectivity of a one-dimensional grid would be close to unity. We observe more complicated behavior, due to the fact that we actually have a two-dimensional grid. When *E* is parallel to the long axis of the grid, or nearly so, we observe significant mode coupling and a weak ESR signal. A similar argument also explains why *E* parallel to the short axis of the mesh is a mode-coupling region. Thus, the optimum orientation is expected and observed to be at an intermediate orientation. We also observe that in the absence of a mesh, the signal is very weak (approximately two orders of magnitude lower and exhibiting significant dispersion).

6 Discussion

Our experience indicates that a brick-wall asymmetric mesh with an aspect ratio of 3:1 is a reasonable choice for many applications. The limiting case of a wire grid is not suitable for cw ESR work, due to the effect of field modulation on a non-rigid structure, although it might have some advantages for pulse work, as discussed by Smith et al. [12]. For less rigid meshes, e.g., copper mesh with a thickness of 0.001 in., we found that microphonic noise is very significant, with an amplitude on the lock-in amplifier of $\sim$1 mV instead of the $\sim$10 μV achievable with the stainless steel mesh. When the sample holder (3 in Fig. 1) with modulation coils (5 in Fig. 1) is too close to the mesh, e.g., mesh number 3, additional noise is observed, due to magnetic field-induced eddy currents that couple via the Lorentz force equation to the magnetic field. This will reduce the SNR, due to baseline instability, if the signal amplitude does not change.

For the low-loss spin-doped dried starch sample, the observed spectra are close to the rigid-limit spectrum, as shown in Fig. 4, and there is broad confirmation of the phase and amplitude dependence as a function of the orientation angle. For this case, however, the phase is less stable in regions of optimal coupling, since mode suppression by loss mechanisms is less effective, and the signal is maximized at a different reference angle. For the aqueous sample, the signal maxima occur at 0° and 110° (corresponding to ±55° from the long axes), where the origin of the phase is explained above. For the low-loss sample, the maxima occur at 0° and 50° (corresponding to ±25° with respect to the long axes). We attribute this to the very different load impedances presented by the lossy and non-lossy samples, parameterized by Z_L, leading to a correspondingly different Z_M necessary for critical coupling [see Eq. (1)].

The resonance response corresponding to the optimal coupling region can be seen on an oscilloscope as the source frequency is swept. In order to tune the spectrometer, a narrow frequency sweep was performed around the resonance frequency. The millimeter wave frequency response of the spectrometer was detected by a hot-electron bolometer and displayed on the oscilloscope. As the bolometer is alernating-current coupled, the frequency sweep or some other time-dependent modulation is necessary to observe an output. In the mode-coupling region, no good resonance is observed. For this reason, the initial orientation was taken to be in the optimal coupling range. By careful positioning of both the sample and upper curved mirror, it is quite easy to put the dip of the resonance on a frequency marker, which indicates the working frequency during spectral acquisition. The resonator resonance should be made as narrow as possible by optimizing the sample position and curved mirror position for a given grid orientation. This procedure yields good spectra, analogous to the optimum SNR shown in, e.g., Fig. 5 or Fig. 6.

Once a good resonant mode has been achieved, small adjustments may be made to the sample position, curved mirror position, and with care, the grid orientation. Due to the relative stability of the phase, once the resonator is well-tuned, one may fine tune the position of the curved mirror to achieve spectra that are nearly pure absorption, so that post-detection phase corrections are minor or unnecessary.

We have also observed that using an asymmetric mesh there is a wider range of sample thickness yielding nearly optimal SNR than what was described earlier [20]. We speculate that the capability to optimize the coupling, even in the presence of a highly lossy sample, allows us to surmount the limitations implied by prior experience [20].

As noted above, sample thickness is not easily correlated with SNR. We have observed that the optimal coupling angle does depend on the sample thickness. Using the same asymmetric mesh, we have been able to critically couple aqueous sample volumes, ranging from 150 nl to 2–3 μl. Although most of the work reported here was performed at 170 GHz, we have also undertaken investigations at 95 and 240 GHz. We determined, e.g., that the experimentally measured sensitivity at 240 GHz from a motionally narrowed 30 μM OH-TEMPO sample is 5×10^7 spins/G, an improvement by a factor of 2 over previous work [20]. For these experiments, the sample volume was 154 nl. The lock-in time constant was 1 s. Interestingly, at

240 GHz, we find that a square mesh gave comparable performance to an asymmetric mesh. We note that the square mesh is easier to use than the asymmetric mesh at 240 GHz in our hands, as the asymmetric mesh has coupling properties that are extremely sensitive to small changes in orientation at this frequency for these small samples.

We have also recently explored the performance of an asymmetric mesh at 95 GHz for cw operation and have demonstrated much improved baseline stability due to the suppression of eddy current-induced microphonics. In addition to the improved baseline stability, we have measured a SNR enhancement of 5.3:1 with the rigid asymmetric mesh, compared to the original, continuously variable symmetric double mesh, which we attribute to microphonics.

We attribute the difference in behavior at 240 GHz compared to 95 and 170 GHz to the difference in the polarization profile of the quasioptical beam across the aperture of corrugated waveguide taper at the input to the resonator [6]. Our simulation software does not currently allow for position-dependent polarization profiles across an aperture. We are thus unable to rigorously explore this conjectured effect theoretically. It is a plausible origin for the experimentally observed behavior, however. We are also currently assessing the importance of imperfections in the mesh fabrication process at the shorter wavelengths.

7 Conclusions

The use of variable-reflectivity meshes as the coupling mechanism for our FPR has allowed us to significantly increase the sensitivity of our high-field high-frequency spectrometers. At 95 GHz, the SNR enhancement is 5.3:1. At 170 GHz, the SNR enhancement is 7:1. At 95 and 170 GHz, we have found that an asymmetric mesh provides the best mix of robustness and performance. At 240 GHz, symmetric meshes give comparable performance to asymmetric meshes and are easier to use in practice than asymmetric meshes. These are critical considerations for the successful investigation of the lossy, concentration-limited samples we study. The results reported here may also be useful in other applications of quasioptics, e.g., microwave spectroscopy or radioastronomy.

Acknowledgments We thank Curt Dunnam for useful discussions. This work was supported by National Institute of Health and National Center for Research Resources (grant nr. 5P41RR016292). K.A.E. was partially supported by a Faculty Research Award Program grant from the University at Albany (SUNY).

References

1. B. Dzikovski, D.S. Tipikin, V. Livshits, K. Earle, J.H. Freed, Phys. Chem. Chem. Phys. (2009). doi: 10.1039/b903490k
2. K.A. Earle, J.H. Freed, Appl. Magn. Reson. **16**, 247–272 (1999)
3. K.A. Earle, B. Dzikovski, W. Hofbauer, J.K. Moscicki, J.H. Freed, Magn. Reson. Chem. **43**, S256–S266 (2005)

4. W. Hofbauer, K.A. Earle, C.R. Dunnam, J.K. Moscicki, J.H. Freed, Rev. Sci. Instrum. **75**(5), 1194–1208 (2004)
5. Z. Liang, Y. Lou, J.H. Freed, L. Columbus, W.L. Hubbell, J. Phys. Chem. **108**, 17649–17659 (2004)
6. P.F. Goldsmith, *Quasioptical Systems. Gaussian Beam Quasioptical Propagation and Applications* (IEEE Press, New York, 1998)
7. Ya.S. Lebedev, in *Modern Pulsed and Continuos-Wave Electron Spin Resonance*, ed. by L. Kevan, M. Bowman (Wiley, New York, 1990), pp. 365–404
8. O. Burghaus, M. Rohrer, T. Götzinger, K. Möbius, Meas. Sci. Technol. **3**, 765–884 (1992)
9. R.T. Weber, J.A.J.M. Disselhorst, L.J. Prevo, J. Schmidt, W.Th. Wenckebach, J. Magn. Reson. **81**, 129 (1989)
10. W.B. Lynch, K.A. Earle, J.H. Freed, Rev. Sci. Instrum. **59**, 1345–1351 (1988)
11. K.A. Earle, D.S. Tipikin, J.H. Freed, Rev. Sci. Instrum. **67**, 2502–2513 (1996)
12. G.M. Smith, J.C.G. Lesurf, R.H. Mitchell, P.C. Riedi, Rev. Sci. Instrum. **69**, 3924–3937 (1998)
13. J.T. Cardin, J.R. Anderson, S.V. Kolaczkowski, D.E. Budil, Appl. Magn. Reson. **16**, 273–292 (1999)
14. J. van Tol, L.C. Brunel, R.J. Wylde, Rev. Sci. Instrum. **76**(7), 074101-1–074101-8 (2005)
15. M.R. Fuchs, T.F. Prisner, K. Möbius, Rev. Sci. Instrum. **70**, 3681–3683 (1999)
16. H. Blok, J.A.J.M. Disselhorst, H. van der Meer, S.B. Orlinskii, J. Schmidt, J. Magn. Reson. **173**(1), 49–53 (2005)
17. J.H. Freed, Ann. Rev. Phys. Chem. **51**, 655–689 (2000)
18. K.A. Earle, D.E. Budil, J.H. Freed, Adv. Mag. Opt. Reson. **19**, 253–325 (1999)
19. J.P. Barnes, J.H. Freed, Rev. Sci. Instrum. **69**, 3022–3027 (1998)
20. R.E. Collin, *Field Theory of Guided Waves*, 2nd edn. (IEEE Press, Newark, 1991)
21. D.E. Budil, Z. Ding, G.R. Smith, K. Earle, J. Magn. Reson. **144**, 20–34 (2000)
22. A. Abragam, *The Principles of Nuclear Magnetism* (Clarendon Press, Oxford, 1961)